Generation of circularly polarized XUV and soft-x-ray high-order harmonics by homonuclear and heteronuclear diatomic molecules subject to bichromatic counter-rotating circularly polarized intense laser fields

John Heslar, Dmitry A. Telnov, and Shih-I Chu

Generation of circularly polarized XUV and soft X-ray high-order harmonics by homonuclear and heteronuclear diatomic molecules subject to bichromatic counter-rotating circularly polarized intense laser fields

John Heslar,[1] Dmitry A. Telnov,[2, *] and Shih-I Chu[1, 3, †]

[1]*Center for Quantum Science and Engineering, and Center for Advanced Study in Theoretical Sciences,*
Department of Physics, National Taiwan University, Taipei 10617, Taiwan
[2]*Department of Physics, St. Petersburg State University,*
7-9 Universitetskaya nab., St. Petersburg 199034, Russia
[3]*Department of Chemistry, University of Kansas, Lawrence, Kansas 66045, USA*

Recently, studies of bright circularly polarized high-harmonic beams from atoms in the soft X-ray region as a source for X-ray magnetic circular dichroism measurement in a tabletop-scale setup have received considerable attention. In this paper, we address the problem with molecular targets and perform a detailed quantum study of H_2^+, CO, and N_2 molecules in bichromatic counter-rotating circularly polarized laser fields where we adopt wavelengths (1300 nm and 790 nm) and intensities (2×10^{14} W/cm^2) reported in a recent experiment [Proc. Natl. Acad. Sci. U.S.A. 595 **112**, 14206 (2015)]. Our treatment of multiphoton processes in homonuclear and heteronuclear diatomic molecules is nonperturbative and based on the time-dependent density functional theory for multielectron systems. The calculated radiation spectrum contains doublets of left and right circularly polarized harmonics with high-energy photons in the XUV and soft X-ray range. Our results reveal intriguing and substantially different nonlinear optical responses for homonuclear and heteronuclear diatomic molecules subject to circularly polarized intense laser fields. We study in detail the below- and above-threshold harmonic regions and analyze the ellipticity and phase of the generated harmonic peaks.

I. INTRODUCTION

High-order-harmonic generation (HHG) is an attractive table-top source of coherent, bright, and tunable extreme ultraviolet (XUV) and soft X-ray radiation with applications in coherent diffractive imaging, ultrafast holography, and time resolved measurements [1–6]. Moreover, circularly polarized HHG may find additional applications in nanolithography, ultrafast spin dynamics, and magnetic circular dichroism [1, 7–13].

However, until recently bright HHG was limited to linear polarization due to the difficulty of controlling elliptically and circularly polarized harmonics and their efficiency. When an atom or molecule is driven by a laser field with slightly elliptical polarization, the electron has some probability of re-colliding with its parent ion it was initially released from, and this results in the generation of harmonics with slight elliptical polarization. However, the HHG efficiency drops drastically with increasing ellipticity of the driving field compared to the case of linearly polarized harmonics generated from linearly polarized laser radiation [14, 15]. In contrast, for circularly polarized driving lasers, the probability of re-collision and the emission of high harmonics is completely suppressed.

A direct approach for generating circularly polarized HHG was suggested 22 years ago [16, 17], and recently measured by Fleischer *et al.* [7]. In this scheme, circularly polarized HHG are driven by co-propagating circularly polarized bichromatic fields that rotate in opposite directions (counter-rotating) and interact with argon gas. This experiment [7] opened up the possibility and motivation of generating bright circularly polarized HHG comparable to the flux efficiency of linearly polarized HHG. Recently, Fan *et al.* [1] did just that, they generated bright circularly polarized soft X-ray HHG beams with photon energies greater than 160 eV and flux comparable to the HHG flux obtained using linearly polarized 800 nm driving lasers. These bright circularly polarized high-order-harmonic beams in the soft X-ray region were generated from He, Ne, and Ar atoms, and used to implement X-ray magnetic circular dichroism measurements in a tabletop-scale setup [1]. Previously, such radiation has only been available at large-scale X-ray facilities such as synchrotrons.

Bright circularly polarized soft X-ray high-order-harmonic beams generated by atomic gases have been used in recent experimental studies to probe magnetic materials, such as the M-shell absorption edges of Co [12], and $N_{4,5}$ absorption edges of Gd [1]. The experiments validated the high degree of circularity, brightness, and stability of this light source [1, 12].

While an impressive progress has been achieved in generation of bright circularly polarized XUV and soft X-ray radiation by atomic targets, this area remains largely unexplored for molecular systems. In this work, we show that generation of bright XUV and soft X-ray radiation with circular polarization is also possible in diatomic molecules. We perform an *all-electron* nonperturbative investigation of multiphoton processes of homonuclear (H_2^+ and N_2) and heteronuclear (CO) diatomic molecules in bichromatic counter-rotating circularly polarized intense laser fields. The H_2^+ molecule is the simplest two-

center one-electron quantum system and is used in our current study as a prototype diatomic molecule to show clearly the physical effects in the generation of circularly polarized harmonics. Then we proceed and take a look at many-electron homonuclear (N_2) and heteronuclear (CO) diatomic molecules. The H_2^+, CO, and N_2 molecules all generate circularly polarized harmonics with photon energies exceeding 160 eV. We also find qualitatively different nonlinear optical response behaviors for homonuclear and heteronuclear diatomic molecules subject to circularly polarized intense laser fields.

The organization of this paper is as follows. In Sec. II we briefly describe the time-dependent density functional (TDDFT) formalism for the general treatment of the multiphoton dynamics of heteronuclear and homonuclear diatomic molecular systems subject to bichromatic counter-rotating circularly polarized intense laser fields. In Sec. III we explore the multiphoton ionization dynamics of H_2^+, CO and N_2 molecules in detail and describe the difference of the ionization process between homonuclear and heteronuclear diatomic molecules. In Sec. IV we study HHG of H_2^+, CO and N_2 molecules driven by bichromatic counter-rotating circularly polarized laser pulses. The HHG spectra for all three molecular systems exhibit a distinct doublet structure, and the harmonics within each doublet possess circular polarizations with opposite handedness. In Sec. V we provide a proof of perfect circular polarization and opposite handedness of the harmonics within the doublets, by calculating their ellipticity and phase parameters from the dipole acceleration data for below- and above-threshold HHG regions. Section VI contains concluding remarks.

II. TIME-DEPENDENT NONPERTURBATIVE TREATMENT OF DIATOMIC MOLECULES IN BICHROMATIC CIRCULARLY POLARIZED LASER PULSES

Detailed numerical procedures we used for the calculation of the H_2^+ molecule can be found in Refs. [18–22]. Also, a more in-depth numerical procedure for the TDDFT of diatomic molecules can be found in Refs. [5, 23–28]. The basic equations of TDDFT are the time-dependent one-electron Kohn-Sham equations [29] for spin orbitals $\psi_{i\sigma}(\boldsymbol{r},t)$ which involve an effective potential $v_{\text{eff},\sigma}(\boldsymbol{r},t)$ (atomic units $\hbar = m = e = 1$ are used unless stated otherwise),

$$i\frac{\partial}{\partial t}\psi_{i\sigma}(\boldsymbol{r},t) = \left[-\frac{1}{2}\nabla^2 + v_{\text{eff},\sigma}(\boldsymbol{r},t)\right]\psi_{i\sigma}(\boldsymbol{r},t),$$
$$i = 1, 2, ..., N_\sigma, \tag{1}$$

where $N_\sigma(= N_\uparrow$ or $N_\downarrow)$ is the total number of electrons for a given spin σ, and the total number of electrons in the system is $N = \sum_\sigma N_\sigma$. The time-dependent effective potential $v_{\text{eff},\sigma}(\boldsymbol{r},t)$ is a functional of the electron spin-densities $\rho_\sigma(\boldsymbol{r},t)$ which are related to the spin orbitals as

follows:

$$\rho_\sigma(\boldsymbol{r},t) = \sum_{i=1}^{N_\sigma} |\psi_{i\sigma}(\boldsymbol{r},t)|^2, \tag{2}$$

(the summation includes all spin orbitals with the same spin). The effective potential $v_{\text{eff},\sigma}(\boldsymbol{r},t)$ in Eq. (1) can be written in the following general form

$$v_{\text{eff},\sigma}(\boldsymbol{r},t) = v_{\text{H}}(\boldsymbol{r},t) + v_{\text{ext}}(\boldsymbol{r},t) + v_{\text{xc},\sigma}(\boldsymbol{r},t), \tag{3}$$

where

$$v_{\text{H}}(\boldsymbol{r},t) = \int \frac{\rho(\boldsymbol{r}',t)}{|\boldsymbol{r} - \boldsymbol{r}'|}d\boldsymbol{r}', \tag{4}$$

is the Hartree potential due to electron-electron Coulomb interaction and $\rho(\boldsymbol{r},t)$ is the total electron density,

$$\rho(\boldsymbol{r},t) = \sum_\sigma \rho_\sigma(\boldsymbol{r},t). \tag{5}$$

$v_{\text{ext}}(\boldsymbol{r},t)$ is the "external" potential due to the interaction of the electron with the external laser fields and the nuclei. In the case of homonuclear or heteronuclear diatomic molecules in bichromatic laser fields, we have

$$v_{\text{ext}}(\boldsymbol{r},t) = v_n(\boldsymbol{r}) + (\boldsymbol{E}_1(t) + \boldsymbol{E}_2(t)) \cdot \boldsymbol{r}, \tag{6}$$

where $v_n(\boldsymbol{r})$ is the nuclear potential,

$$v_n(\boldsymbol{r}) = -\frac{Z_1}{|\boldsymbol{R}_1 - \boldsymbol{r}|} - \frac{Z_2}{|\boldsymbol{R}_2 - \boldsymbol{r}|}, \tag{7}$$

with Z_1 and Z_2 being the electric charges of the two nuclei and $\boldsymbol{R}_1$ and $\boldsymbol{R}_2$ being their coordinates at the fixed equilibrium positions. The internuclear separation R is equal to $|\boldsymbol{R}_2 - \boldsymbol{R}_1|$. The laser electric field strengths $\boldsymbol{E}_1(t)$ and $\boldsymbol{E}_2(t)$ refer to the two frequency components of the bichromatic field. We assume that the laser fields $\boldsymbol{E}_1(t)$ and $\boldsymbol{E}_2(t)$ are polarized in the $x-y$ plane with the molecular axis directed along the z axis. Finally, $v_{\text{xc},\sigma}(\boldsymbol{r},t)$ is the time-dependent exchange-correlation (xc) potential. Since the exact form of $v_{\text{xc},\sigma}(\boldsymbol{r},t)$ is unknown, the *adiabatic* approximation is often used [23–27, 30]

$$v_{\text{xc},\sigma}(\boldsymbol{r},t) = v_{\text{xc},\sigma}[\rho_\sigma]|_{\rho_\sigma = \rho_\sigma(\boldsymbol{r},t)}. \tag{8}$$

When these potentials, determined by the time-independent ground-state density functional theory (DFT), are used along with TDDFT in the electronic structure calculations, both inner shell and excited states can be calculated rather accurately [31]. In this work, we utilize the improved van Leeuwen-Baerends LBα xc potential [32]. The LBα contains two empirical parameters α and β and has the following explicit form, in the adiabatic approximation,

$$v_{\text{xc},\sigma}^{\text{LB}\alpha}(\boldsymbol{r},t) = \alpha v_{\text{x},\sigma}^{\text{LSDA}}(\boldsymbol{r},t) + v_{\text{c},\sigma}^{\text{LSDA}}(\boldsymbol{r},t)$$
$$-\frac{\beta x_\sigma^2(\boldsymbol{r},t)\rho_\sigma^{1/3}(\boldsymbol{r},t)}{1 + 3\beta x_\sigma(\boldsymbol{r},t)\ln\{x_\sigma(\boldsymbol{r},t) + [x_\sigma^2(\boldsymbol{r},t) + 1]^{1/2}\}}. \tag{9}$$

Here, ρ_σ is the electron density with spin σ, and we use $\alpha = 1.19$ and $\beta = 0.01$ [24–27]. The first two terms in Eq. (9), $v_{\mathrm{x},\sigma}^{\mathrm{LSDA}}$ and $v_{\mathrm{c},\sigma}^{\mathrm{LSDA}}$ are the LSDA exchange and correlation potentials that do *not* have the correct Coulombic asymptotic behavior. The last term in Eq. (9) is the nonlocal gradient correction with $x_\sigma(\boldsymbol{r}) = |\nabla \rho_\sigma(\boldsymbol{r})|/\rho_\sigma^{4/3}(\boldsymbol{r})$, which ensures the proper long-range Coulombic asymptotic potential $v_{\mathrm{xc},\sigma}^{\mathrm{LB}\alpha} \rightarrow -1/r$ as $r \rightarrow \infty$. Note that if the conventional xc energy functional forms taken from local spin density approximation (LSDA) or generalized gradient approximation (GGA) [33, 34] are used, the corresponding xc potential $v_{\mathrm{xc},\sigma}(\boldsymbol{r}, t)$ will not possess the correct long-range asymptotic $(-1/r)$ behavior [35]. For the time-independent case, this exchange-correlation LBα potential has been found to be reliable for atomic and molecular DFT calculations [2, 24–27, 32, 36–38].

In what follows, we shall assume that the molecular axis is fixed in space and directed along the Cartesian z-axis. The laser fields propagate along the z-axis and have circular polarizations in the $x - y$ plane. The counter-rotating fields $\boldsymbol{E}_1(t)$ and $\boldsymbol{E}_2(t)$ are expressed as follows:

$$\boldsymbol{E}_1(t) = \frac{1}{\sqrt{2}} F_1(t) \left[\hat{\boldsymbol{e}}_x \cos(\omega_1 t) + \hat{\boldsymbol{e}}_y \sin(\omega_1 t) \right], \quad (10)$$

$$\boldsymbol{E}_2(t) = \frac{1}{\sqrt{2}} F_2(t - \Delta\tau) \left[\hat{\boldsymbol{e}}_x \cos(\omega_2 t - \Delta\tau) - \hat{\boldsymbol{e}}_y \sin(\omega_2 t - \Delta\tau) \right]. \quad (11)$$

$\Delta\tau$ presents the time delay between the two pulses, $\boldsymbol{E}_1(t)$ and $\boldsymbol{E}_2(t)$. Since the dipole approximation is well justified in the near infrared wavelength region, the fields are assumed uniform in space. In Eqs. (10) and (11), ω_1 and ω_2 denote the carrier frequencies while $F_1(t)$ and $F_2(t)$ represent the temporal pulse envelopes, We use the sine-squared pulse shape:

$$F_1(t) = F_0 \sin^2 \frac{\pi t}{N_1 T_1}, \quad (12)$$

$$F_2(t) = F_0 \sin^2 \frac{\pi t}{N_2 T_2}, \quad (13)$$

where F_0 is the peak electric field strength (we use the same peak field strength for both fields), T_1 and T_2 are the optical cycle durations for each field $[T_1 = 2\pi/\omega_1$ and $T_2 = 2\pi/\omega_2]$, and the integer numbers N_1 and N_2 are the total pulse durations measured in optical cycles.

Solution of the time-dependent Schrödinger (H_2^+) and one-electron Kohn-Sham (N_2 and CO) equations for two-center systems is greatly facilitated in the prolate spheroidal coordinates. The relationship between the prolate spheroidal coordinates ξ, η, φ and Cartesian coordinates x, y, z is as follows:

$$x = \frac{1}{2} R \sqrt{(\xi^2 - 1)(1 - \eta^2)} \cos\varphi, \quad (14)$$
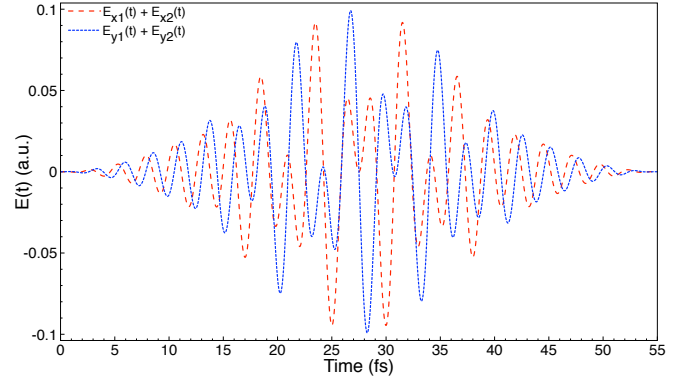

FIG. 1. (Color online) Time-dependent electric field of the driving laser pulse. The red dotted and blue dashed lines represent the electric field in the x and y direction, respectively. The laser pulse has a duration of 21 optical cycles (~ 55 fs) for the ω_1 (790 nm) component and 8 optical cycles (~ 35 fs) for the ω_2 (1300 nm) component. The time delay $\Delta\tau \sim 11$ fs. Both frequency components have the same peak field strength corresponding to the intensity of 2×10^{14} W/cm^2.

$$y = \frac{1}{2} R \sqrt{(\xi^2 - 1)(1 - \eta^2)} \sin\varphi, \quad (15)$$

$$z = \frac{1}{2} R \xi \eta, \quad (16)$$

where R is the internuclear distance. The dipole interaction potentials in the length gauge have the following expressions in the prolate spheroidal coordinates:

$$\boldsymbol{E}_1(t) \cdot \boldsymbol{r} = \frac{R}{2\sqrt{2}} F_1(t) \sqrt{(\xi^2 - 1)(1 - \eta^2)} \left[\cos\phi \cdot \cos(\omega_1 t) + \sin\phi \cdot \sin(\omega_1 t) \right], \quad (17)$$

$$\boldsymbol{E}_2(t) \cdot \boldsymbol{r} = \frac{R}{2\sqrt{2}} F_2(t - \Delta\tau) \sqrt{(\xi^2 - 1)(1 - \eta^2)} \\ \times \left[\cos\phi \cdot \cos(\omega_2 t - \Delta\tau) - \sin\phi \cdot \sin(\omega_2 t - \Delta\tau) \right]. \quad (18)$$

In Eqs. (10)-(18), $F_1(t)$ and $F_2(t)$ denote the laser pulse envelope functions, ω_1 and ω_2 are the carrier frequencies. Here, for the counter-rotating circularly polarized pulses, left-helicity corresponds to 790 nm pulse $[\boldsymbol{E}_1(t)]$ and right-helicity corresponds to the 1300 nm pulse $[\boldsymbol{E}_2(t)]$.

In our calculations, we use the carrier wavelengths 790 nm for the field $\boldsymbol{E}_1(t)$ ($\omega_1 = 0.0576$ a.u.= 1.57 eV) and 1300 nm for the field $\boldsymbol{E}_2(t)$ ($\omega_2 = 0.0350$ a.u.= 0.95 eV), respectively. The peak field strength F_0 corresponds to the intensity 2×10^{14} W/cm^2. The pulse durations are chosen as $N_1 = 21$ and $N_2 = 8$, and the time delay $\Delta\tau \sim 11$ fs, which makes $\boldsymbol{E}_1(t)$ and $\boldsymbol{E}_2(t)$ symmetric about their common center (see Fig. 1). To

discretize the 3D wave function in coordinate space and propagate it in time, we apply the time-dependent generalized pseudospectral method (TDGPS) [39]. The time-dependent Schrödinger (for the H_2^+ molecule) and Kohn-Sham (for N_2 and CO molecules) equations are solved by means of the second-order split-operator technique in prolate spheroidal coordinates and in the energy representation. To obtain fairly converged HHG spectra for the laser field parameters used in the calculations, we set the grid size (for ξ, η, and φ coordinates, respectively) to $96 \times 32 \times 16$ and use 4096 time steps per optical cycle in the time propagation process. The linear dimension of the box where the time-dependent equations are solved is chosen as 43 a.u.; between 23 and 43 a.u. we apply an absorber which smoothly brings down the propagated wave functions without spurious reflections from the boundary. With this box size, all important physics is well described for the laser field parameters used in the calculations, although some very long trajectories (in the semiclassical picture of HHG) may be missing. Of course, a larger box size is better but it also requires a larger number of grid points to maintain the same accuracy level of the computed orbitals in the core spatial region, which is emphasized when calculating the HHG spectra in the acceleration form. The total linear dimension of the propagator matrix for the current grid is 49152, which is already very large, and its substantial increase would make the computations impractical.

The HHG power spectra can be investigated accurately once the time-dependent Kohn-Sham orbitals and total electron density $\rho(\boldsymbol{r}, t)$ are available. We calculate the expectation values of the induced dipole acceleration in the x, y, and z directions:

$$a_x(t) = \int d^3r \; \rho(\boldsymbol{r}, t) \frac{\partial v_{\mathrm{n}}}{\partial x} + E_{1x}(t) + E_{2x}(t), \quad (19)$$

$$a_y(t) = \int d^3r \; \rho(\boldsymbol{r}, t) \frac{\partial v_{\mathrm{n}}}{\partial y} + E_{1y}(t) + E_{2y}(t), \quad (20)$$

$$a_z(t) = \int d^3r \; \rho(\boldsymbol{r}, t) \frac{\partial v_{\mathrm{n}}}{\partial z}. \quad (21)$$

Then the power spectra $S(\omega)$ (spectral density of the radiation energy) can be obtained by the Fourier transformation of the time-dependent dipole accelerations,

$$S_x(\omega) = \frac{2}{3\pi c^3} \left| \int_{-\infty}^{\infty} a_x(t) \exp(i\omega t) dt \right|^2, \quad (22)$$

$$S_y(\omega) = \frac{2}{3\pi c^3} \left| \int_{-\infty}^{\infty} a_y(t) \exp(i\omega t) dt \right|^2, \quad (23)$$

$$S_z(\omega) = \frac{2}{3\pi c^3} \left| \int_{-\infty}^{\infty} a_z(t) \exp(i\omega t) dt \right|^2, \quad (24)$$

$$S_{\mathrm{tot}}(\omega) = S_x(\omega) + S_y(\omega) + S_z(\omega). \quad (25)$$

III. MULTIPHOTON IONIZATION OF H_2^+, N_2 AND CO MOLECULES IN BICHROMATIC CIRCULARLY POLARIZED LASER PULSES

The ground-state electronic configurations is $1\sigma_g^1$ for H_2^+, $1\sigma_g^2 1\sigma_u^2 2\sigma_g^2 2\sigma_u^2 1\pi_u^4 3\sigma_g^2$ for N_2 and $1\sigma^2 2\sigma^2 3\sigma^2 4\sigma^2 1\pi^4 5\sigma^2$ for CO, respectively. The highest occupied molecular orbital (HOMO) for H_2^+, N_2, and CO is $1\sigma_g$, $3\sigma_g$, and 5σ, respectively. N_2 and CO are isoelectronic molecules, both having 14 electrons and triple bonds. Since the CO molecule has unequal nuclear charges, its ground electronic state possesses a permanent dipole moment, calculated here to be 0.149 Debye. The corresponding experimental value is 0.112 Debye [40]. Furthermore, there is no concept of gerade and ungerade orbitals for CO (or any other heteronuclear diatomic molecule) since the inversion symmetry of the potential is broken. An important difference between the H_2^+ and N_2 and CO spectra is that the latter contain even as well as odd harmonics [5, 24–27]. Generation of even harmonics is forbidden in systems with inversion symmetry, such as atoms and homonuclear diatomic molecules. This selection rule does not apply to the heteronuclear molecules with no inversion center (CO).

Once the time-dependent wave functions and the time-dependent electron densities are obtained, we can calculate the time-dependent (multiphoton) ionization probability of an individual spin-orbital according to

$$P_{i,\sigma} = 1 - N_{i,\sigma}(t), \quad (26)$$

where

$$N_{i,\sigma}(t) = \langle \psi_{i,\sigma}(\xi, \eta, \varphi, t) | \psi_{i,\sigma}(\xi, \eta, \varphi, t) \rangle, \quad (27)$$

is the time-dependent population (survival probability) of the $i\sigma$-th spin-orbital.

Figure 2 presents the time-dependent population of individual spin orbital, as defined in Eq. (27). The slope of the decay of the electron population in time determines the ionization rate. The internuclear distance for H_2^+ ($R_e = 2.000a_0$), CO ($R_e = 2.132a_0$), and N_2 ($R_e = 2.072a_0$) molecules is fixed at its equilibrium distance R_e. Results for the counter-rotating laser intensities ($F_0 = 2 \times 10^{14}$ W/cm^2) and wavelengths of $\lambda_1 = 790$ nm and $\lambda_2 = 1300$ nm are shown for H_2^+, N_2 and CO molecules. In Figs. 2(a-c) the laser pulses have a time duration of 21 optical cycles for ω_1 (790 nm) and 8 optical cycles for ω_2 (1300 nm). The calculated ionization potentials for H_2^+, CO, and N_2 molecules are 1.1026 a.u. [19], 0.5093 a.u.[5], and 0.5682 a.u.[5], respectively. The multiphoton ionization in the circularly polarized laser fields is dominated by the HOMO, that is $1\sigma_g$ in H_2^+, 5σ in CO, and $3\sigma_g$ in N_2. The ionization probability of H_2^+ (Fig. 2(a)) is much lower than that of CO (Fig. 2(b)) and N_2 (Fig. 2(c)), since the H_2^+ molecules ionization potential is almost twice that of CO and N_2 ionization potentials. The orbital structure and ionization potentials of CO and N_2 are close to each other. One would

expect similar behaviors from CO and N$_2$ molecules in laser fields with the same wavelength and intensity, but we previously proved this is not true [27]. In intense low-frequency laser fields, the multiphoton ionization occurs mainly in the tunneling regime. In this picture, the ionization takes place in the DC field with slow varying amplitude from zero to its peak value. The width of the potential barrier depends on the field strength; the stronger the field, the narrower the barrier. Thus the ionization occurs mainly at the peak values of the field strength. The probability of tunneling ionization is very sensitive with respect to the HOMO energy. However, in the external field this energy is changed due to the Stark shift. The nitrogen molecule is symmetric with respect to inversion, that is why the Stark shift in a DC field is quadratic in the field strength and the N$_2$ molecules HOMO energy differs slightly (0.0001 a.u.) from its unperturbed value [27]. On the contrary, the carbon monoxide molecule has a permanent dipole moment, and the DC Stark shift is linear in the field strength; at the peak values of the field, the HOMO energy can differ significantly (~ 0.1 a.u.) from its unperturbed value [27]. In our previous studies of CO and N$_2$ in a linear polarized laser field with the same wavelength and intensity the ionization probability of CO is much larger than that of N$_2$ [26, 27]. In Figs. 2(b) (CO molecule) and 2(c) (N$_2$ molecule) we observe the same phenomena in bichromatic counter-rotating circularly polarized laser pulses, the ionization probability of CO is much larger than that of N$_2$. We also note that ionization of CO is dominated by HOMO while in N$_2$ both HOMO and HOMO-1 have comparable ionization probabilities. This is well explained by the ionization potentials of HOMO-1 in these molecules. The ionization potential of HOMO-1 in N$_2$ is only 1.4 eV larger than that of HOMO; in CO, the energy difference between HOMO and HOMO-1 is twice as large, 3.2 eV.

IV. CIRCULARLY POLARIZED HIGH-ORDER HARMONICS IN H$_2^+$, N$_2$ AND CO MOLECULES

The observed HHG spectra in Figs. 3-5 can be described in terms of the energy and angular momentum conservation in the process of absorption of the driving fields photons and emission of the harmonic photon. [1, 6, 7, 13, 16, 41]. The energy conservation gives $\omega_c = n_1\omega_1 + n_2\omega_2$ for the frequency ω_c of the emitted photon after absorption of n_1 photons of frequency ω_1 and n_2 photons of frequency ω_2. The angular momentum conservation requires $n_2 = n_1 \pm 1$ for the circularly-polarized counter-rotating driving fields $\boldsymbol{E}_1$ and $\boldsymbol{E}_2$. Then the emitted photon frequency can be represented as $\omega_c = (2n+1)(\omega_1 + \omega_2)/2 \pm (\omega_1 - \omega_2)/2$, n being a positive integer number. This gives rise to a doublet structure of the HHG spectrum, with the frequency differences $\omega_1 + \omega_2$ between the adjacent doublets and $\omega_1 - \omega_2$ between the photon emission peaks within
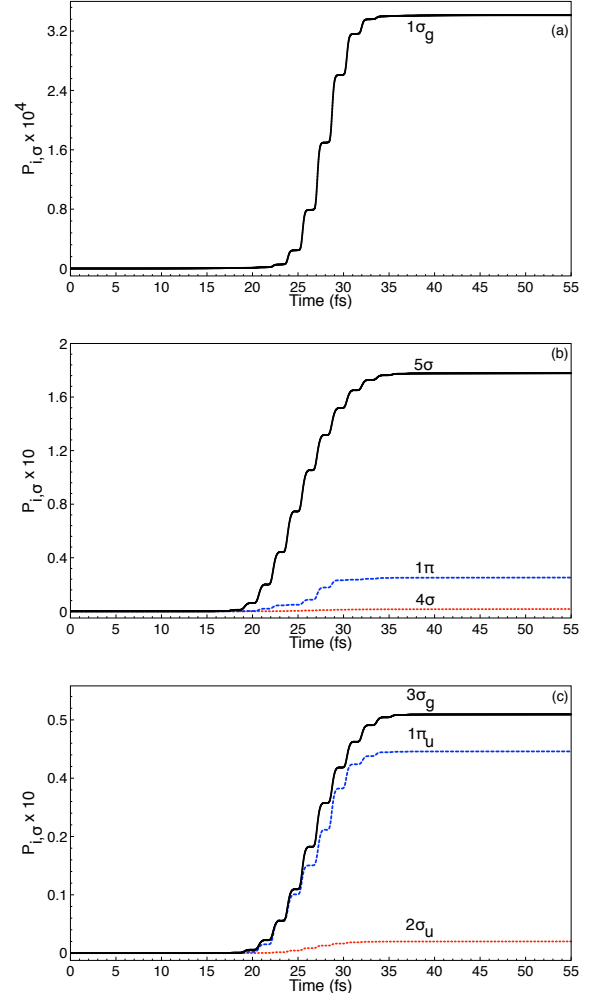

FIG. 2. (Color online) The time-dependent ionization probability of electrons in different spin orbital's of (a) H$_2^+$, (b) CO, and (c) N$_2$ molecules in the counter-rotating circularly polarized laser pulses. The laser pulses have a time duration of 21 optical cycles (~ 55 fs) for ω_1 (790 nm) and 8 optical cycles (~ 35 fs) for ω_2 (1300 nm). The time delay $\Delta\tau \sim 11$ fs.

the same doublet. The right peak in the doublet has a circular polarization with the same helicity as the driving field with the higher frequency ($\boldsymbol{E}_1$), the left peak has a circular polarization with the same helicity as the driving field with the lower frequency ($\boldsymbol{E}_2$). If we define $\omega_1 = q\omega_2$, where q can be any number, we obtain $\omega_c = n_1(q+1)\omega_2 \pm \omega_2$. For the driving laser wavelengths studied here (790 and 1300 nm), $\omega_c = (2.65n_1 \pm 1)\omega_2$.

While the calculated HHG spectra for H$_2^+$ and N$_2$ in Figs. 3 and 5, respectively, show the peak positions match well those predicted by the selection rules and specified above, the CO spectrum in Fig. 4 has extra peaks corresponding to even harmonics with $n_1 = n_2$. Generation of such harmonics is forbidden in atoms and homonuclear diatomic molecules where the energy levels have definite

parity due to the inversion symmetry. Only the states with the opposite parities are coupled by the dipole interaction (one-photon emission and absorption), therefore absorption of an even number of photons $n_1 + n_2$ cannot be followed by emission of a single photon. This restriction is lifted for oriented heteronuclear diatomic molecules. For the present scheme with two counterrotating circularly polarized driving fields, generation of even harmonics is only possible if $n_1 = n_2$, otherwise conservation of the angular momentum projection does not allow for the photon emission. The excitation of the molecule with absorption of $n_1 = n_2$ photons, however, does not change the angular momentum projection on the z axis, thus the emitted even harmonic photon cannot be circularly polarized in the $x - y$ plane. We will discuss polarization of emitted radiation in detail below in Sec. V.

In Fig. 3, we present the HHG spectrum of H_2^+ for the driving laser pulse shown in Fig. 1. The spectrum displays harmonics with photon energies up to ~ 160 eV. The ionization threshold (I_p) for the initially occupied $1\sigma_g$ molecular orbital is marked with the green dashed vertical line at 29.9 eV. Figure 3(b) shows the below- and near-threshold region. As one can see, almost all the peaks in the spectrum exhibit a clear doublet structure with the spacing between the main peaks equal to $\omega_1 + \omega_2$ and subpeak separation of $\omega_1 - \omega_2$. According to the general considerations discussed above, the components of the doublet (subpeaks within each main peak) must have circular polarizations opposite to each other. Fig. 3(c) shows the above-threshold harmonics up to photon energies of ~ 110 eV. Here the doublet structure of the harmonics is not so distinct as in the below-threshold region, especially for the photon energies larger than 80 eV. We can suggest the following explanation of this observation. High-order harmonics are predominantly generated at times when the laser field reaches its highest strength, that is near the center of the laser pulse. In the vicinity of the time moment t_0, corresponding to the half duration of the laser pulse ($t_0 \approx 27.5$ fs, see Fig. 1), the x and y components of the laser electric field (10)–(11) can be approximated as

$$
\begin{aligned}
E_x(t) = F_0\sqrt{2}\sin\left[\frac{1}{2}(\omega_1 - \omega_2)(t - t_0)\right] \\
\times \sin\left[\frac{1}{2}(\omega_1 + \omega_2)(t - t_0)\right],
\end{aligned}
\tag{28}
$$

$$
\begin{aligned}
E_y(t) = -F_0\sqrt{2}\cos\left[\frac{1}{2}(\omega_1 - \omega_2)(t - t_0)\right] \\
\times \sin\left[\frac{1}{2}(\omega_1 + \omega_2)(t - t_0)\right].
\end{aligned}
\tag{29}
$$

When the frequency difference $\omega_1 - \omega_2$ is small, the component $E_y(t)$ is larger than $E_x(t)$ and approximately represents a monochromatic field with the frequency $(\omega_1 + \omega_2)/2$. For the current choice of the laser field parameters, this is clearly seen in Fig. 1 for the optical cycle
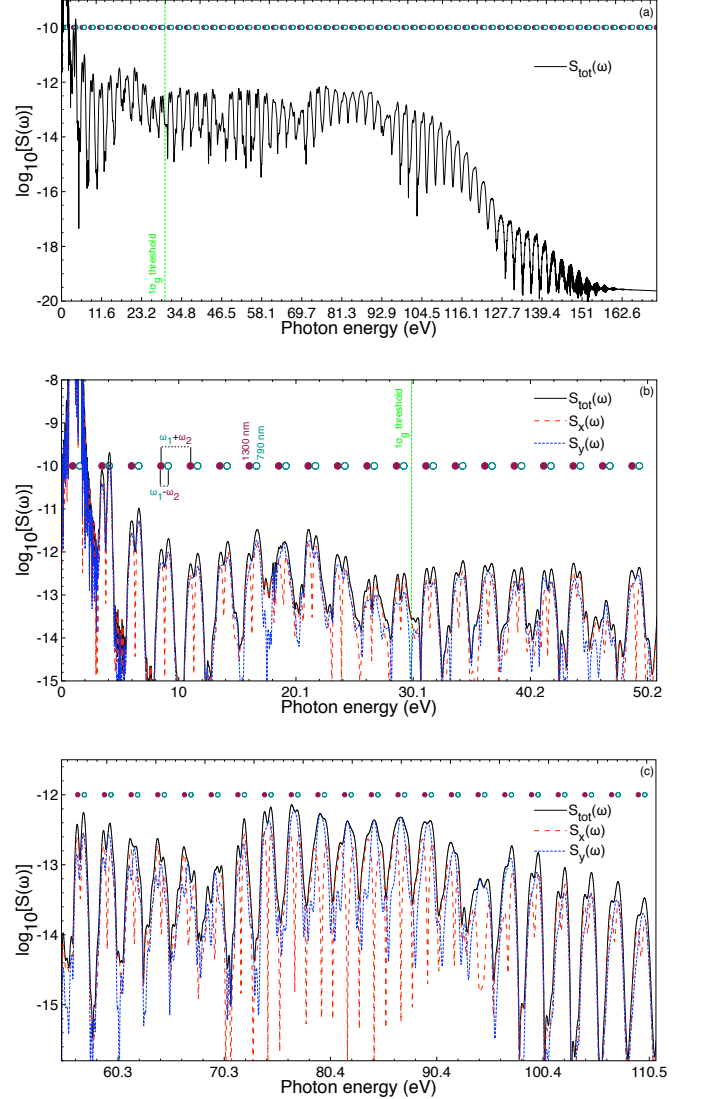

FIG. 3. (Color online) HHG spectrum $S(\omega)$ in the x, y, and total domain of the H_2^+ molecule in the counter-rotating circularly polarized laser pulses. Circularly polarized XUV and soft X-ray HHG spectrum (a) up to ~ 160 eV, (b) below- and near-threshold, and (c) above-threshold. The laser pulses have a time duration of 21 optical cycles for ω_1 (790 nm) and 8 optical cycles for ω_2 (1300 nm). The green vertical dashed line indicates the corresponding ionization threshold (I_p) marked by $1\sigma_g$ threshold. All spectra show a doublet structure, located at positions predicted by energy and spin angular momentum conservation [filled maroon circles (1300 nm) and open teal circles (790 nm)]. The separation within each doublet is $\omega_1 - \omega_2$, and different doublets are separated by $\omega_1 + \omega_2$.

in the center of the laser pulse. Consequently, one can expect a dominant contribution from the y component of the dipole acceleration to the harmonic signal in the high-energy part of the HHG spectrum. This is indeed the case, as one can see in Fig. 3(c). Since the two-color

nature of $E_y(t)$ is less pronounced in the vicinity of the time moment t_0, the doublet structure of the total HHG spectrum is less distinct for higher harmonic orders. The situation will change for the different choice of the laser filed parameters, such as frequencies and time delay between the fields $\boldsymbol{E}_1(t)$ and $\boldsymbol{E}_2(t)$. For example, one may expect a more distinct doublet structure in high-order harmonics for the larger difference between ω_1 and ω_2.

Next, we show the CO molecule (Fig. 4) where it also has odd order circularly polarized harmonics with photon energies up to ~ 160 eV. The laser pulse parameters for the CO molecule are the same as those for the H_2^+ molecule in Fig. 3. The ionization threshold (I_p) for the 5σ orbital (HOMO) is marked with the green dashed vertical line at 13.9 eV. Figure 4(b) shows the below- and near-threshold region where the doublets separated from each other by the frequency $\omega_1 + \omega_2$ and containing two harmonics with opposite circular polarizations split by the photon energy of $\omega_1 - \omega_2$ are clearly seen and labeled. Figure. 4(c) shows the above-threshold harmonics up to photon energies of ~ 65 eV. An important difference between the H_2^+ (Fig. 3) and CO (Fig. 4) spectra is that the latter contain even as well as odd harmonics. Generation of even harmonics is forbidden in systems with inversion symmetry, such as atoms and homonuclear diatomic molecules. This selection rule does not apply to the heteronuclear molecules with no inversion center (CO). This can be clearly seen in the below- and near-threshold harmonic region in Fig. 4(b), where the extra peaks (even harmonics) lie between the adjacent doublets of odd harmonics. Unlike the doublets of the odd harmonics, the even harmonics are linearly polarized as they are generated solely by the dipole acceleration along the z axis. For example, one can see an even harmonic peak at the photon energy $\omega_c = 20.7$ eV in Fig. 4(b), that lies between the adjacent doublets (labeled by the filled maroon circles and open teal circles) of odd harmonics.

Intuitively, one expects that the driving field polarized in the x (or y, or z) direction induces the dipole moment in the *same* direction. However, this is true only for symmetric systems such as atoms and homonuclear diatomic molecules where the polarization tensor is diagonal (with z being the molecular axis in the case of diatomic molecules). This intuitive picture is invalid for heteronuclear diatomic molecules where the charge distribution has no inversion symmetry with respect to the center of the molecule. Then the force acting perpendicular to the molecular axis (in the x or y direction) would cause a non-symmetric charge displacement along the z-axis as well, inducing a dipole moment in this direction. Unlike the permanent dipole moment of a heteronuclear molecule along the molecular axis, this induced dipole moment would oscillate with the driving field thus generating harmonics polarized in the z direction. This phenomenon can be clearly observed in Fig. 4(b), where the HHG spectrum has a non-zero contribution $S_z(\omega)$ due to the dipole acceleration in the z direction. This contribution is responsible for generation of even harmonics
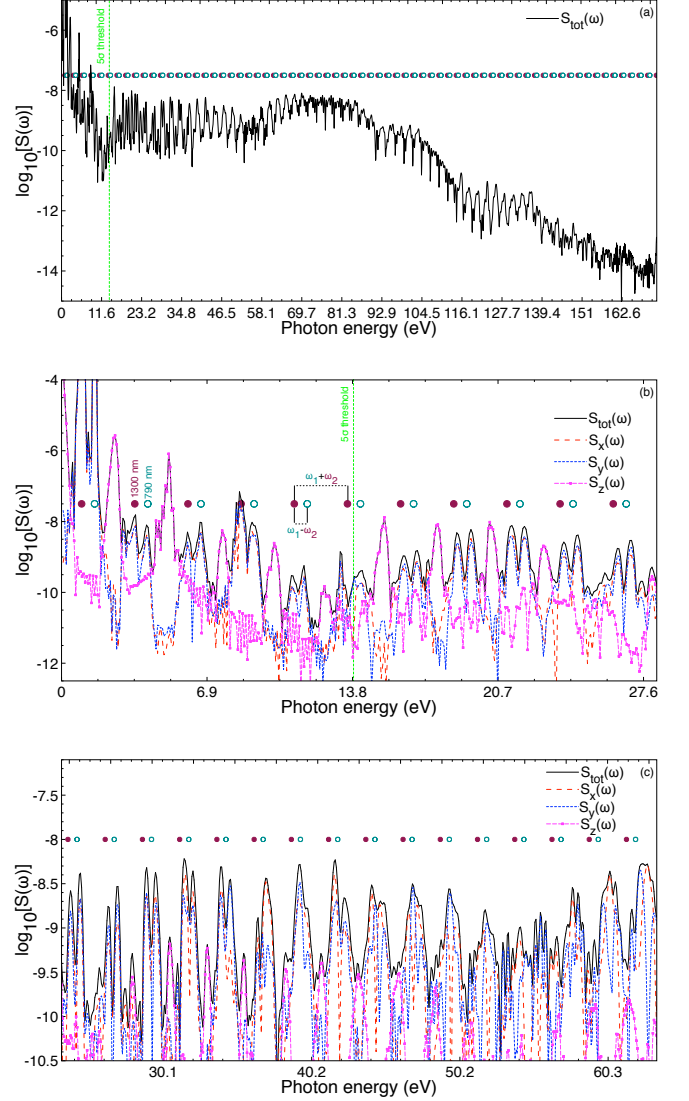

FIG. 4. (Color online) HHG spectrum $S(\omega)$ in the x, y, z, and total domain of the CO molecule in the counter-rotating circularly polarized laser pulses. Circularly polarized XUV and soft X-ray HHG spectrum (a) up to ~ 170 eV, (b) below- and near-threshold, and (c) above-threshold. The laser pulses have a time duration of 21 optical cycles for ω_1 (790 nm) and 8 optical cycles for ω_2 (1300 nm). The green vertical dashed line indicates the corresponding HOMO ionization threshold (I_p) marked by 5σ threshold. All spectra show a doublet structure, located at positions predicted by energy and spin angular momentum conservation [filled maroon circles (1300 nm) and open teal circles (790 nm)]. The separation within each doublet is $\omega_1 - \omega_2$, and different doublets are separated by $\omega_1 + \omega_2$.

linearly polarized along the z axis (n_1 must be equal to n_2 because of conservation of the angular momentum projection: a dipole accelerated along the z axis can only emit photons with zero spin projection on this axis). Other contributions to the HHG spectrum, $S_x(\omega)$ and $S_y(\omega)$,
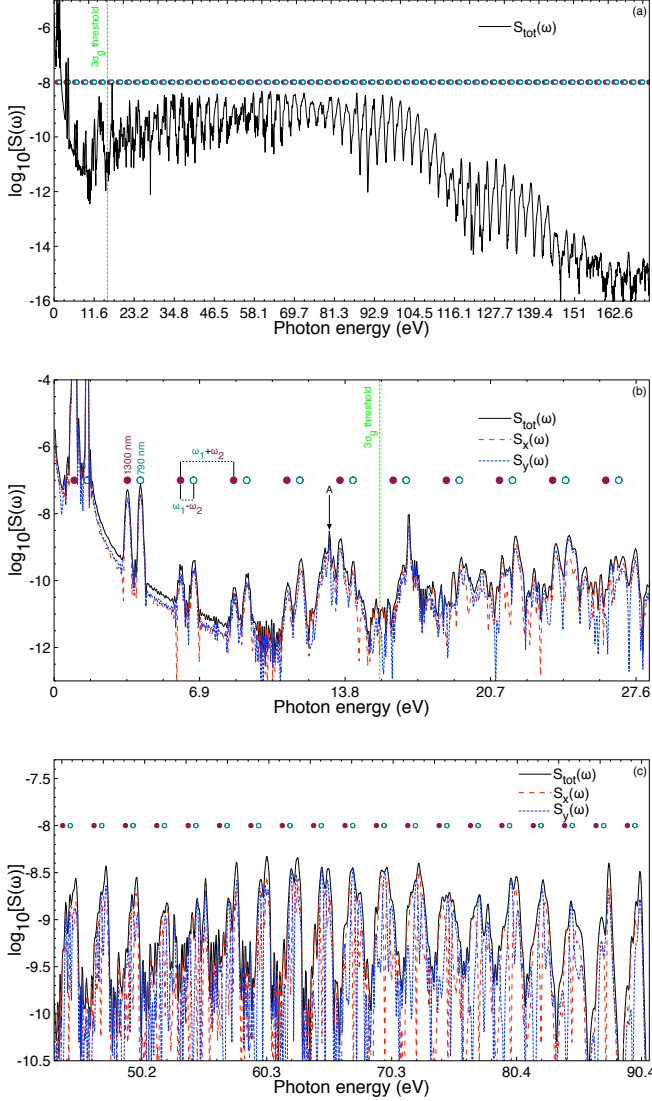
FIG. 5. (Color online) HHG spectrum $S(\omega)$ in the x, y, and total domain of the N_2 molecule in the counter-rotating circularly polarized laser pulses. Circularly polarized XUV and soft X-ray HHG spectrum (a) up to ~ 170 eV, (b) below- and near-threshold, and (c) above-threshold. The laser pulses have a time duration of 31 optical cycles for ω_1 (790 nm) and 12 optical cycles for ω_2 (1300 nm). Resonance A in panel (b) corresponds to the $3\sigma_g - 2\pi_u$ and $3\sigma_g - 3\sigma_u$ excited-state resonance peaks. The green vertical dashed line indicates the corresponding HOMO ionization threshold (I_p) marked by $3\sigma_g$ threshold. All spectra show a doublet structure, located at positions predicted by energy and spin angular momentum conservation [filled maroon circles (1300 nm) and open teal circles (790 nm)]. The separation within each doublet is $\omega_1 - \omega_2$, and different doublets are separated by $\omega_1 + \omega_2$.

are responsible for generation of harmonic doublets with circular polarizations in the $x - y$ plane. A qualitative difference between the HHG processes in homonuclear and oriented heteronuclear molecules is, therefore, not only in the fact of generation of even harmonics by heteronuclear molecules. Polarization of even harmonics is also different: it is linear and directed along the molecular axis while the driving fields and odd harmonics are polarized in the plane perpendicular to the molecular axis. As one can see in Fig. 4, even harmonics are strong only for low orders (up to ~ 35 eV), and then the signal $S_z(\omega)$ becomes much weaker than the signals $S_x(\omega)$ and $S_y(\omega)$ of odd harmonics. This is not surprising since the natural scale of the plateau region, suggested by the famous semiclassical three-step model [42] and based on the ponderomotive energy, does not apply to the harmonic radiation generated by the dipole oscillations in the z direction where no direct force from the driving laser field is present. Only Coulomb forces from the nuclei and other electrons can cause oscillations of the particular orbital electron density in this direction. During these oscillations, the electron cannot gain a large kinetic energy before recombining with the molecular core and emitting the harmonic photon, unlike the case of motion in the x and y directions under direct influence from the laser field. Consequently, the HHG spectrum of even harmonics exhibits a shorter plateau region than that in the spectrum of odd harmonics.

Finally, in Fig 5 we show the N_2 molecule where it also has circularly polarized harmonics with photon energies up to ~ 160 eV. In Fig. 5 the laser pulses have a time duration of 31 optical cycles (~ 82 fs) for ω_1 (790 nm) and 12 optical cycles (~ 52 fs) for ω_2 (1300 nm) and the laser fields both have a peak intensity of $F_0 = 2 \times 10^{14}$ W/cm^2 [Eqs. (12)-(13)]. A longer pulse duration is used for the N_2 molecule to make the doublets containing harmonics with opposite circular polarizations (split by $\omega_1 - \omega_2$) more structured and well shaped. The N_2 molecule also produces circularly polarized harmonics with photon energies up to ~ 160 eV. The ionization threshold (I_p) for the $3\sigma_g$ orbital (HOMO) is marked with the green dashed vertical line at 15.5 eV. Figure 5(b) shows the below- and near-threshold region where the doublets separated from each other by the frequency $\omega_1 + \omega_2$ and containing two harmonics with opposite circular polarizations split by the photon energy of $\omega_1 - \omega_2$ are clearly seen and labeled. Also, two excited-state resonance peaks ($3\sigma_g - 2\pi_u$ and $3\sigma_g - 3\sigma_u$) are labeled "A" at 13 eV in Fig. 5(b). Figure. 5(c) shows the above-threshold harmonics up to photon energies of ~ 160 eV.

V. ELLIPTICITY AND PHASE OF THE CIRCULARLY POLARIZED HARMONIC SIGNALS

Generation of circularly polarized high-order harmonics by bichromatic counter-rotating circularly polarized drivers results in harmonic doublets, where in each doublet the harmonics are circularly polarized with opposite handedness, and can span the XUV and soft X-ray regions. Here, we prove the polarizations of the harmonics
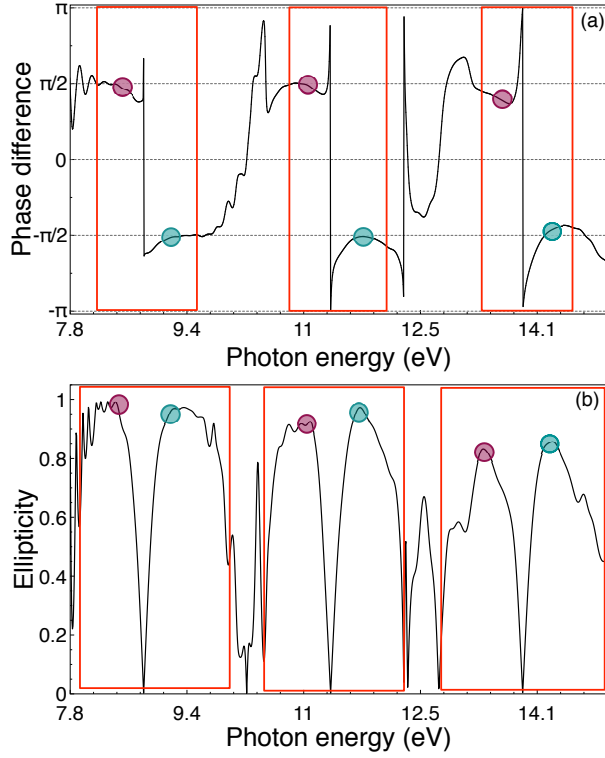
FIG. 6. (Color online) (a) Phase and (b) ellipticity of the harmonic signals $[S_x(\omega) + S_y(\omega)]$ from H_2^+ as a function of photon energy (below-threshold harmonics). The laser parameters used are the same as those in Fig. 3. The filled maroon circles and filled teal circles mark the harmonic peak positions within each doublet. The phases of the harmonics within the same doublet exhibit opposite signs: $\sim \pm\pi/2$.
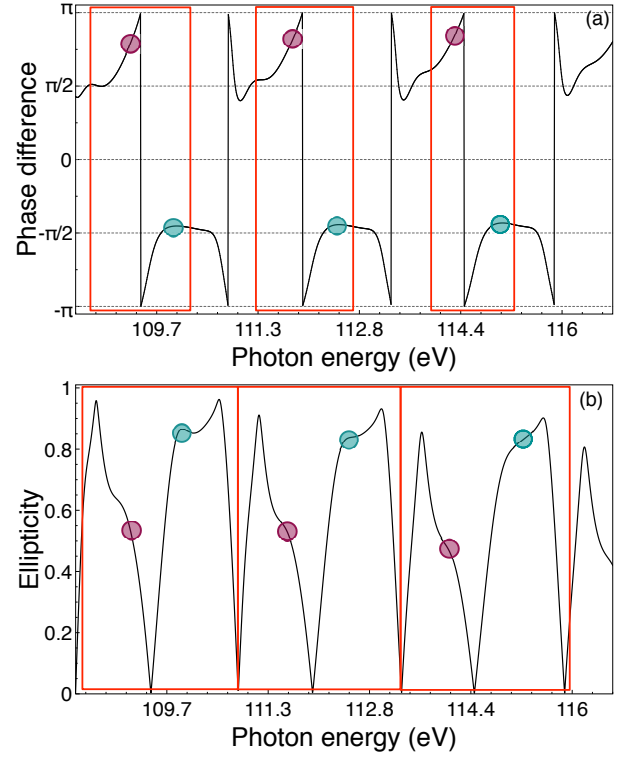

FIG. 7. (Color online) (a) Phase and (b) ellipticity of the harmonic signals $[S_x(\omega) + S_y(\omega)]$ from H_2^+ as a function of photon energy (above-threshold harmonics). The laser parameters used are the same as those in Fig. 3. The filled maroon circles and filled teal circles mark the harmonic peak positions within each doublet.

are the same as those of the frequency components of the driving two-color driving laser field, hence, the harmonics have circular polarizations with left and right handedness.

Suppose we have a monochromatic field with the components along x and y:

$$
\begin{aligned}
F_x &= a\cos(\omega t), \\
F_y &= b\cos(\omega t + \beta).
\end{aligned}
\tag{30}
$$

Generally, the field amplitudes along x and y are different (with their ratio $r_{yx} = b/a$), and there is a phaseshift β between the field oscillations in x and y directions. Actually, Eq. (30) represents an elliptically polarized field; the orientation of the ellipse in the $x - y$ plane depends on the parameters r_{yx} and β. The angle α which determines the orientation of one of the ellipse axes with respect to the x-axis is calculated as:

$$
\alpha = -\frac{1}{2}\arctan\left(\frac{r_{yx}^2 \sin(2\beta)}{1 + r_{yx}^2 \cos(2\beta)}\right).
\tag{31}
$$

The second axis has the orientation angle $\alpha + \pi/2$. Assuming the first axis to be the major axis of the ellipse,

the ellipticity parameter is calculated as follows:

$$
\epsilon = \sqrt{\frac{\sin^2\alpha + r_{yx}^2 \sin^2(\alpha + \beta)}{\cos^2\alpha + r_{yx}^2 \cos^2(\alpha + \beta)}}
\tag{32}
$$

If the calculated ellipticity parameter ϵ appears greater than unity, then the first axis is actually the minor axis, and the ellipticity parameter is given by $1/\epsilon$. From the Fourier transform of the induced dipole acceleration (which represents the harmonic field), one can obtain the parameters r_{yx} and β and calculate the ellipticity for the specific frequency ω. The circular polarization ($\epsilon = 1$) is only possible if $\beta = \pm\pi/2$ and $r_{yx} = 1$.

In Figs. 6-11, the filled maroon circles and filled teal circles indicate the positions of harmonic peaks within each doublet. The circular polarization of the harmonics marked with the teal circles has the same handedness as that of the driving field $\boldsymbol{E}_1(t)$, and the harmonics marked with the maroon circles are polarized with the same handedness as the driving field $\boldsymbol{E}_2(t)$.

Figures 6 (below-threshold region) and 7 (above-threshold region) show the phase and ellipticity of the harmonics in the HHG spectrum of H_2^+ molecule (Fig 3). As one can see in Fig. 6, the ellipticity of the below-threshold harmonics is near unity and the phases are
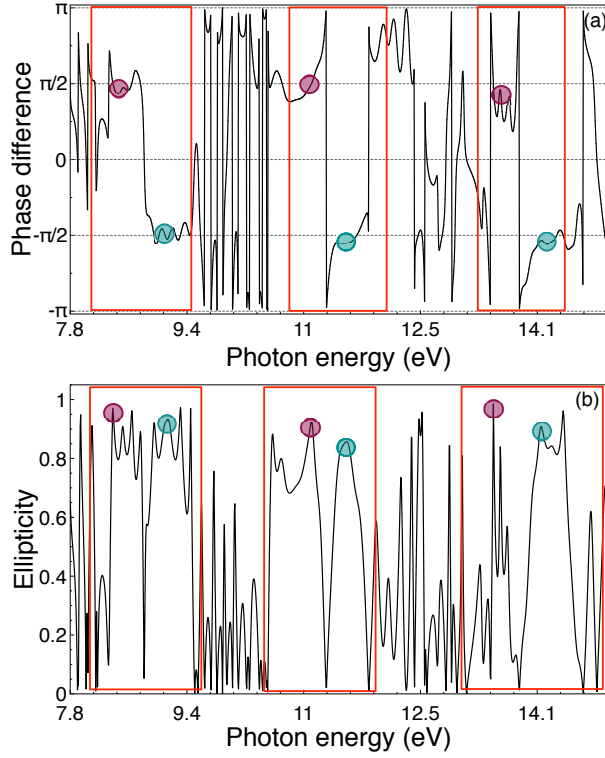
FIG. 8. (Color online) (a) Phase and (b) ellipticity of the harmonic signals $[S_x(\omega) + S_y(\omega)]$ from CO as a function of photon energy (below-threshold harmonics). The laser parameters used are the same as those in Fig. 4. The filled maroon circles and filled teal circles mark the harmonic peak positions within each doublet. The phases of the harmonics within the same doublet exhibit opposite signs: $\sim \pm\pi/2$.
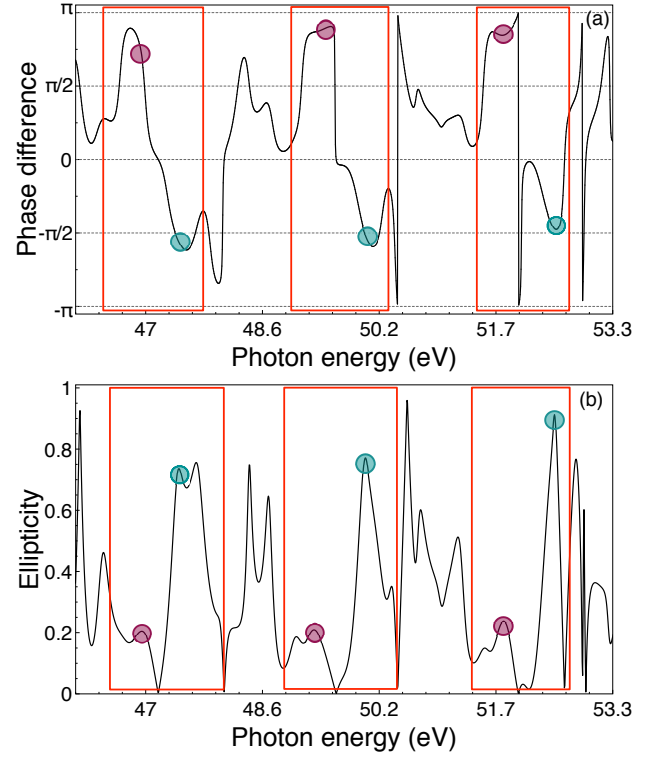

FIG. 9. (Color online) (a) Phase and (b) ellipticity of the harmonic signals $[S_x(\omega) + S_y(\omega)]$ from CO as a function of photon energy (above-threshold harmonics). The laser parameters used are the same as those in Fig. 4. The filled maroon circles and filled teal circles mark the harmonic peak positions within each doublet.

very close to $\pm\pi/2$, indicating circular polarizations with left and right handedness. In the above-threshold region (Fig. 7), the ellipticity and phases start to deviate from the values characterizing perfect circular polarization near the photon energy of ~ 109 eV.

Next, in Figs. 8 (below-threshold region) and 9 (above-threshold region) we show the phase and ellipticity of the harmonics in the HHG spectrum of CO molecule (Fig 4). Here, we analyze only the odd harmonics polarized in the $x - y$ plane, since the even harmonics are linearly polarized along the molecular (z) axis, as it was discussed above. Again, in the below-threshold region (Fig. 8), the harmonics in the same doublet have nearly perfect circular polarization with opposite handedness. In the above-threshold region (Fig. 9), the ellipticity and phases start to deviate from unity and $\pm\pi/2$, respectively, starting from the photon energy of ~ 47 eV.

Figures 10 (below-threshold region) and 11 (above-threshold region) show the phase and ellipticity of the harmonics in the HHG spectrum of N_2 molecule (Fig 5). The picture resembles that previously seen in the H_2^+ and CO molecules. In the below-threshold region, the harmonics have almost perfect circular polarization with the ellipticity equal to unity and phases equal to $\pm\pi/2$ for left

and right handedness. However, in the above-threshold region, the ellipticity eventually drops from unity, and the harmonics do not exhibit circular polarization starting from the photon energy of ~ 60 eV.

VI. CONCLUSION

In this paper, we have presented a detailed investigation and analysis of heteronuclear and homonuclear diatomic molecules subject to bichromatic counter-rotating circularly polarized intense laser fields. The generated high-order harmonics exhibit circular polarization up to the soft x-ray regime for the homonuclear (H_2^+, N_2) and heteronuclear (CO) molecules under consideration. The HHG spectrum has a doublet structure where the harmonics within the same doublet have opposite (left and right) circular polarizations.

We found that qualitatively different nonlinear optical responses and ionization dynamics are predicted for heteronuclear and homonuclear diatomic molecules, although CO has only a very small permanent dipole moment. First, the MPI rate for the heteronuclear diatomic CO molecules is larger than that for H_2^+ and N_2 homonuclear diatomic molecules. Second, while the excitation of
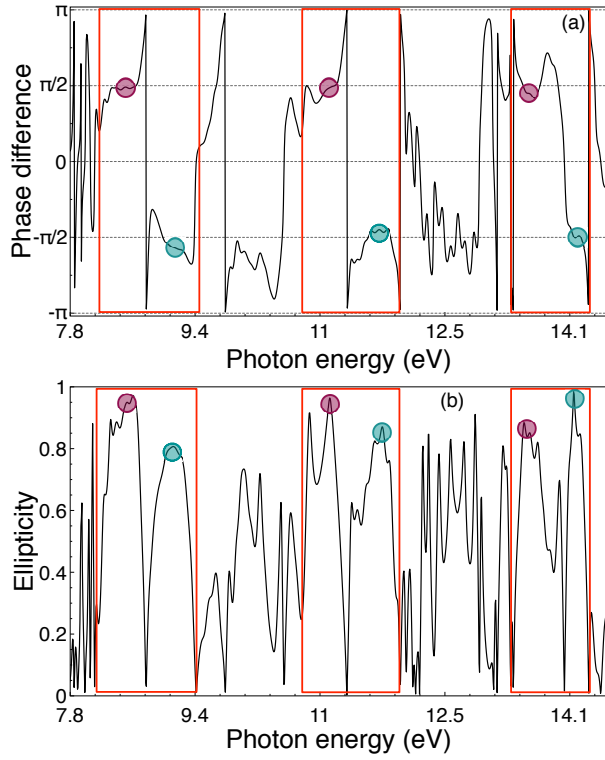
FIG. 10. (Color online) (a) Phase and (b) ellipticity of the harmonic signals $[S_x(\omega) + S_y(\omega)]$ from N_2 as a function of photon energy (below-threshold harmonics). The laser parameters used are the same as those in Fig. 5. The filled maroon circles and filled teal circles mark the harmonic peak positions within each doublet. The phases of the harmonics within the same doublet exhibit opposite signs: $\sim \pm\pi/2$.

the H_2^+ and N_2 molecules by laser fields can generate only odd harmonics, both even and odd harmonics can be produced in the case of oriented CO molecules. Third, for heteronuclear diatomic molecules (CO), the laser fields propagating along the molecular (z) axis and circularly polarized in the perpendicular $x - y$ plane cause a non-symmetric time-dependent displacement of the electron density along the molecular axis thus inducing an oscillating dipole moment in the z direction, although the force from the laser fields does not have a projection on the z axis. Oscillations of the dipole moment along the molecular axis result in generation of even order harmonics, linearly polarized in the same z direction. This HHG mechanism is unavailable in homonuclear diatomic molecules and qualitatively distinguishes harmonic generation in homonuclear and heteronuclear diatomic molecules in circularly polarized laser fields.

Finally, our results show that generation of bright XUV

and soft x-ray radiation with circular polarization is also possible in diatomic molecules and not limited to atomic targets only. Much remains to be explored in this fascinating and largely unexplored area of molecular nonlinear optical processes in strong bichromatic circularly polarized laser fields.
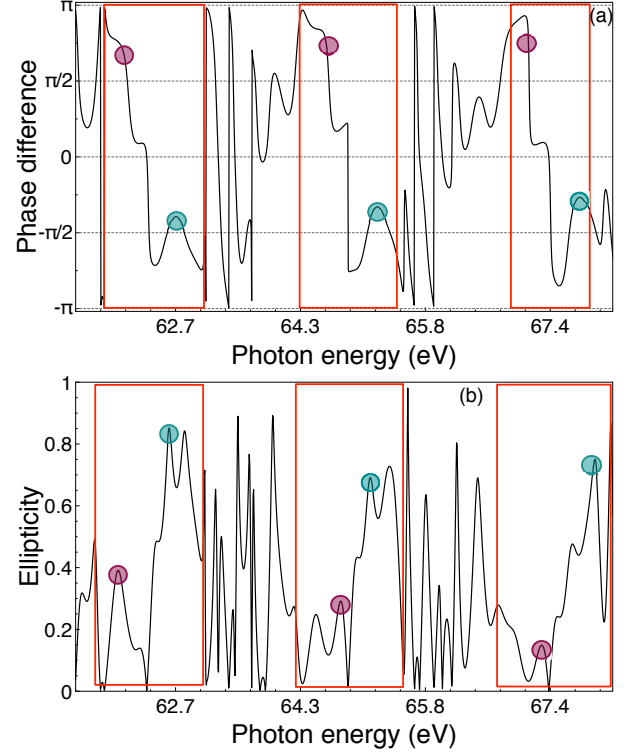

FIG. 11. (Color online) (a) Phase and (b) ellipticity of the harmonic signals $[S_x(\omega) + S_y(\omega)]$ from N_2 as a function of photon energy (above-threshold harmonics). The laser parameters used are the same as those in Fig. 5. The filled maroon circles and filled teal circles mark the harmonic peak positions within each doublet.

ACKNOWLEDGMENTS

[1] T. Fan, P. Grychtol, R. Knut, C. Hernndez-Garca, D. D. Hickstein, D. Zusin, C. Gentry, F. J. Dollar, C. A. Mancuso, C. W. Hogle, et al., Proc. Natl. Acad. Sci. U.S.A. **112**, 14206 (2015).

[2] M. Chini, X. Wang, Y. Cheng, H. Wang, Y. Wu, E. Cunningham, P.-C. Li, J. Heslar, D. Telnov, S. Chu, et al., Nat. Photonics **8**, 437 (2014).

[3] I.-Y. Park, S. Kim, J. Choi, D.-H. Lee, Y.-J. Kim, M. Kling, M. Stockman, and S.-W. Kim, Nat. Photonics **5**, 677 (2011).

[4] S. Kim, J. Jin, Y.-J. Kim, I.-Y. Park, K. Seung-Woo, and S.-W. Kim, Nature **453**, 757 (2008).

[5] J. Heslar, D. A. Telnov, and S. I. Chu, Phys. Rev. A **93**, 063401 (2016).

[6] A. Rundquist, C. G. Durfee, Z. Chang, C. Herne, S. Backus, M. M. Murnane, and H. C. Kapteyn, Science **280**, 1412 (1998).

[7] A. Fleischer, O. Kfir, T. Diskin, P. Sidorenko, and O. Cohen, Nat. Photonics **8**, 543 (2014).

[8] O. Kfir, P. Grychtol, E. Turgut, R. Knut, D. Zusin, A. Fleischer, E. Bordo, T. Fan, D. Popmintchev, T. Popmintchev, et al., J. Phys. B **49**, 123501 (2016).

[9] E. Turgut, C. La-o vorakiat, J. M. Shaw, P. Grychtol, H. T. Nembach, D. Rudolf, R. Adam, M. Aeschlimann, C. M. Schneider, T. J. Silva, et al., Phys. Rev. Lett. **110**, 197201 (2013).

[10] S. Mathias, C. La-O-Vorakiat, P. Grychtol, P. Granitzka, E. Turgut, J. M. Shaw, R. Adam, H. T. Nembach, M. E. Siemens, S. Eich, et al., Proc. Natl. Acad. Sci. U.S.A. **109**, 4792 (2012).

[11] C. La-O-Vorakiat, M. Siemens, M. M. Murnane, H. C. Kapteyn, S. Mathias, M. Aeschlimann, P. Grychtol, R. Adam, C. M. Schneider, J. M. Shaw, et al., Phys. Rev. Lett. **103**, 257402 (2009).

[12] O. Kfir, P. Grychtol, E. Turgut, R. Knut, D. Zusin, D. Popmintchev, T. Popmintchev, H. Nembach, J. M. Shaw, A. Fleischer, et al., Nat. Photonics **9**, 99 (2015).

[13] D. B. Milosevic, J. Phys. B **48**, 171001 (2015).

[14] M. Möller, Y. Cheng, S. D. Khan, B. Zhao, K. Zhao, M. Chini, G. G. Paulus, and Z. Chang, Phys. Rev. A **86**, 011401 (2012).

[15] F. A. Weihe, S. K. Dutta, G. Korn, D. Du, P. H. Bucksbaum, and P. L. Shkolnikov, Phys. Rev. A **51**, R3433 (1995).

[16] S. Long, W. Becker, and J. K. McIver, Phys. Rev. A **52**, 2262 (1995).

[17] H. Eichmann, A. Egbert, S. Nolte, C. Momma, B. Wellegehausen, W. Becker, S. Long, and J. K. McIver, Phys. Rev. A **51**, R3414 (1995).

[18] D. A. Telnov, J. Heslar, and S. I. Chu, Phys. Rev. A **95**, 043425 (2017).

[19] J. Heslar and S. I. Chu, Sci. Rep. **6**, 37774 (2016).

[20] K. N. Avanaki, D. A. Telnov, and S. I. Chu, J. Phys. B **49**, 114002 (2016).

[21] S. K. Son, D. A. Telnov, and S. I. Chu, Phys. Rev. A **82**, 043829 (2010).

[22] D. A. Telnov and S. I. Chu, Phys. Rev. A **76**, 043412 (2007).

[23] X. Chu and S. I. Chu, Phys. Rev. A **63**, 023411 (2001).

[24] D. A. Telnov, J. Heslar, and S. I. Chu, in *Theoretical and Computational Developments in Modern Density Functional Theory*, edited by A. K. Roy (Nova Science Publishers Inc., New York, 2012), Time-Dependent Density Functional Theoretical Methods for Many-Electron Molecular System, pp. 357–390.

[25] J. Heslar, D. A. Telnov, and S. I. Chu, in *Concepts and Methods in Modern Theoretical Chemistry: Statistical Mechanics Volume 2*, edited by S. Ghosh and P. Chattaraj (Taylor and Francis Inc., Bosa Roca, 2013), Time-Dependent Density Functional Theoretical Methods for Nonperturbative Treatment of Multiphoton Processes of Many-Electron Molecular Systems in Intense Laser Fields, pp. 37–55.

[26] J. Heslar, D. A. Telnov, and S. I. Chu, Phys. Rev. A **83**, 043414 (2011).

[27] J. Heslar, J. J. Carrera, D. A. Telnov, and S. I. Chu, Int. J. Quant. Chem. **107**, 3159 (2007).

[28] J. Heslar and S. I. Chu, Phys. Rev. A **95**, 043414 (2017).

[29] W. Kohn and L. J. Sham, Phys. Rev. **140**, A1113 (1965).

[30] C. A. Ullrich, U. J. Gossmann, and E. K. U. Gross, Phys. Rev. Lett. **74**, 872 (1995).

[31] M. A. L. Marques, C. A. Ullrich, F. Nogueira, A. Rubio, K. Burke, and E. K. U. Gross, eds., *Time-Dependent Density Functional Theory* (Springer, Berlin, 2006).

[32] P. R. T. Schipper, O. V. Gritsenko, S. J. A. van Gisbergen, and E. J. J. Baerends, J. Chem. Phys. **112**, 1344 (2000).

[33] R. G. Parr and W. Yang, *Density-Functional Theory of Atoms and Molecules* (Oxford University Press, Oxford, 1989).

[34] R. M. Dreizler and E. K. U. Gross, *Density Functional Theory, An Approach to the Quantum Many-Body Problem* (Springer, Berlin, 1990).

[35] X. M. Tong and S. I. Chu, Phys. Rev. A **55**, 3406 (1997).

[36] S. I. Chu, J. Chem. Phys. **123**, 062207 (2005).

[37] R. van Leeuwn and E. J. Baerends, Phys. Rev. A **49**, 2421 (1994).

[38] D. A. Telnov, J. Heslar, and S. I. Chu, Phys. Rev. A **90**, 063412 (2014).

[39] X. M. Tong and S. I. Chu, Chem. Phys. **217**, 119 (1997).

[40] R. D. Nelson Jr., D. R. Lide, and A. A. Maryott, in *National Standard Reference Data Series* (Natl. Bur. Stand. (U.S.) Circ. No. 10, US GPO, Washington, DC, 1967), Time-Dependent Density Functional Theoretical Methods for Many-Electron Molecular System, p. 1.

[41] E. Pisanty, S. Sukiasyan, and M. Ivanov, Phys. Rev. A **90**, 043829 (2014).

[42] P. B. Corkum, Phys. Rev. Lett. **71**, 1994 (1993).